

**COMMUNICATION**

# Engineering an enhanced voltage-sensing phosphatase

Akira Kawanabe<sup>1</sup> , Natsuki Mizutani<sup>1</sup>, Onur K. Polat<sup>3</sup> , Tomoko Yonezawa<sup>1</sup>, Takafumi Kawai<sup>1</sup>, Masayuki X. Mori<sup>3</sup>, and Yasushi Okamura<sup>1,2</sup> 

**Voltage-sensing phosphatases (VSP) consist of a membrane-spanning voltage sensor domain and a cytoplasmic region that has enzymatic activity toward phosphoinositides (PIs). VSP enzyme activity is regulated by membrane potential, and its activation leads to rapid and reversible alteration of cellular PIP levels. These properties enable VSPs to be used as a tool for studying the effects of phosphatidylinositol-4,5-bisphosphate (PI(4,5)P<sub>2</sub>) binding to ion channels and transporters. For example, by applying simple changes in the membrane potential, *Danio rerio* VSP (Dr-VSP) has been used effectively to manipulate PI(4,5)P<sub>2</sub> in mammalian cells with few, if any, side effects. In the present study, we report an enhanced version of Dr-VSP as an improved molecular tool for depleting PI(4,5)P<sub>2</sub> from cultured mammalian cells. We modified Dr-VSP in two ways. Its voltage-dependent phosphatase activity was enhanced by introducing an aromatic residue at the position of Leu-223 within a membrane-interacting region of the phosphatase domain called the hydrophobic spine. In addition, selective plasma membrane targeting of Dr-VSP was facilitated by fusion with the N-terminal region of *Ciona intestinalis* VSP. This modified Dr-VSP (CiDr-VSP<sup>mChe</sup> L223F, or what we call eVSP) induced more drastic voltage-evoked changes in PI(4,5)P<sub>2</sub> levels, using the activities of Kir2.1, KCNQ2/3, and TRPC6 channels as functional readouts. eVSP is thus an improved molecular tool for evaluating the PI(4,5)P<sub>2</sub> sensitivity of ion channels in living cells.**

Phosphoinositides (PIs) are essential components of membrane lipids in eukaryotes. In addition, they play a number of fundamental roles in cell signaling. For example, PIs directly activate downstream signaling molecules, such as kinases, through their binding to PI-recognizing domains. PIs also serve as precursors to intracellular second messengers and transcellular lipid mediators (Balla, 2013), and they bind to and regulate the activities of diverse membrane proteins. Phosphatidylinositol-4,5-bisphosphate (PI(4,5)P<sub>2</sub>) is the most abundant PI in the plasma membrane and is known to regulate the activities of various ion channels, transporters, and receptors (Hille et al., 2015). Other PIs, including PI(3,5)P<sub>2</sub>, PI(3,4)P<sub>2</sub>, PI(3,4,5)P<sub>3</sub>, also regulate ion channel activities (Samie et al., 2013; She et al., 2019; Shimomura and Kubo, 2019). Indeed, recent structural biological analyses revealed the PI-containing structures of ion channels whose sensitivity to PIs had not been previously known (Laverty et al., 2019), which implies that regulation of ion channels by PIs is more widespread than previously thought. However, the physiological significance of PI regulation of ion channels and transporters largely remains to be determined. Clarification

must await detailed quantitative comparison of PI sensitivity among these proteins.

To study the PI(4,5)P<sub>2</sub> sensitivity of ion channels and transporters in living cells, several molecular tools, which alter the amount of PI(4,5)P<sub>2</sub> within biological membranes by activating relevant enzymes using chemical compounds, light, or voltage, are available (Balla, 2013; Hille et al., 2015). A classical example of manipulation of PI metabolism using a chemical reagent is heterologous expression of a G protein-coupled receptor, muscarinic acetylcholine receptor type 1, which binds acetylcholine to induce activation of PLC, leading to cleavage of PI(4,5)P<sub>2</sub> into two signaling molecules: diacylglycerol and inositol-trisphosphate. Another commonly used approach is to induce membrane targeting of PI-related enzymes through dimerization of FK506 binding protein (FKBP) and mTOR (FRB), mediated by rapamycin or its analogue, iRap. Application of rapamycin or iRap induces recruitment of a FKBP-bound PI-related enzyme to a target membrane through binding to membrane-anchored FRB. Although this is a versatile method useful for any cytoplasmic enzyme, membrane recruitment and the appearance of enzyme

<sup>1</sup>Laboratory of Integrative Physiology, Department of Physiology, Graduate School of Medicine, Osaka University, Suita, Osaka, Japan; <sup>2</sup>Graduate School of Frontier Biosciences, Osaka University, Suita, Osaka, Japan; <sup>3</sup>Department of Synthetic Chemistry and Biological Chemistry, Graduate School of Engineering, Kyoto University, Kyoto, Japan.

Correspondence to Yasushi Okamura: [yokamura@phys2.med.osaka-u.ac.jp](mailto:yokamura@phys2.med.osaka-u.ac.jp); A. Kawanabe's present address is Molecular Physiology and Biophysics, Faculty of Medicine, Kagawa University, Miki-cho, Kagawa, Japan; M.X. Mori's present address is Bio-materials and Chemistry, University of Occupational and Environmental Health, Fukuoka, Japan.

© 2020 Kawanabe et al. This article is distributed under the terms of an Attribution–Noncommercial–Share Alike–No Mirror Sites license for the first six months after the publication date (see <http://www.rupress.org/terms/>). After six months it is available under a Creative Commons License (Attribution–Noncommercial–Share Alike 4.0 International license, as described at <https://creativecommons.org/licenses/by-nc-sa/4.0/>).

activity take more than seconds, and the induction is irreversible. In another system, membrane recruitment of PI-related enzymes is induced through CRY2 dimerization under light control (Idevall-Hagren et al., 2012). This enables manipulation of plasma membrane PI(4,5)P<sub>2</sub> levels with high spatial resolution. Again, however, temporal resolution is limited, since the CRY2-containing enzyme needs to translocate from the cytoplasm to the membrane.

Voltage-sensing phosphatase (VSP) is a uniquely effective tool for analyzing the PI(4,5)P<sub>2</sub> sensitivity of membrane proteins thanks to its robust ability to deplete PI(4,5)P<sub>2</sub> upon simple manipulation of the membrane voltage. VSP has several advantages over the other tools mentioned. First, VSP shows rapid activation in response to depolarizing stimulation. Second, heterologous expression of a single VSP polypeptide is sufficient to induce voltage-dependent PI phosphatase activity; no supplemental material is required. Third, the recovery process following VSP-catalyzed PI(4,5)P<sub>2</sub> depletion can be examined upon simple repolarization of the membrane voltage. This is in contrast to the rapamycin-inducible enzyme system, which produces irreversible depletion of PIs. PI sensitivity has been studied using VSP in ~30 species of membrane proteins so far (Falkenburger et al., 2010; Suh et al., 2010; Thornell and Bevensee, 2015; Okamura et al., 2018; Mizutani et al., 2019). However, ion channels with very high binding affinity for PIs may not be easily studied using the current version of VSP. This is because complete depletion of PIs using VSP may require very high or prolonged membrane depolarization, which often causes deterioration of the cell's state.

To address that issue, we designed an enhanced version of VSP based on *Danio rerio* VSP (Dr-VSP). Dr-VSP has been frequently used to estimate the PI(4,5)P<sub>2</sub> sensitivity of ion channels in cultured mammalian cells (Suh et al., 2010; Imai et al., 2012; Kruse et al., 2012; Hille et al., 2015; Okamura et al., 2018). We enhanced the voltage-dependent enzyme activity of Dr-VSP by introducing an amino acid mutation at a recently identified site of interface between the membrane and the phosphatase domain, which we call the “hydrophobic spine.” This site plays critical roles in both the intrinsic phosphatase activity and the voltage-enzyme coupling of *Ciona intestinalis* VSP (Ci-VSP; Kawanabe et al., 2018). The structure of the hydrophobic spine is highly conserved among VSP orthologues and even phosphatase and tensin homologue deleted from chromosome 10 (PTEN). The corresponding region in Dr-VSP consists of Leu-223 and Tyr-224. In the present study, we show that L223F mutation enhances the voltage-dependent enzyme activity of Dr-VSP, indicating that the function of the hydrophobic spine is conserved between Dr-VSP and Ci-VSP. Second, membrane targeting of Dr-VSP was facilitated by attaching the N-terminal cytoplasmic segment of Ci-VSP, which is known to mediate targeting to plasma membrane (Tsutsui et al., 2013). These two modifications of Dr-VSP provided the enzyme with enhanced voltage-dependent phosphatase activity. We anticipate that this enhanced version of Dr-VSP (eVSP) will serve as a useful tool for examining the PI(4,5)P<sub>2</sub> dependence of membrane proteins.

## Materials and methods

### cDNAs and in vitro mutagenesis

The following cDNAs were used for expression in culture cells (HEK293T): Dr-VSP in pIRES2-EGFP (Hossain et al., 2008); mouse-Kir2.1 (Kir2.1) in pCXN2 (kindly provided by Y. Kubo, National Institute for Physiological Sciences, Okazaki, Japan); KCNQ2-YFP and KCNQ3-YFP (kindly provided by B. Hille, University of Washington, Seattle, WA); and human TRPC6 (available from GenBank under accession no. NM\_004621) in pcDNA3 provided by T. Hofmann and M. Schaefer (Institut für Pharmakologie und Toxikologie, Würzburg, Germany).

Point mutations at Leu-223 in Dr-VSP were generated using a Quik Change Site-Directed Mutagenesis kit (Stratagene) or PrimeSTAR Mutagenesis Basal kit (Takara Bio). To produce mCherry-tagged constructs, the cDNA for Dr-VSP was amplified by PCR and ligated into a customized pcDNA3.1(-) (Invitrogen) expression vector, which yielded mCherry fused at the C-terminal end of the target protein (Dr-VSP<sup>mCherry</sup>). Chimeric proteins composed of Ci-VSP (M1-G103) and Dr-VSP (Q44-P511; CiDr-VSP) were generated through two-step PCR and ligated into the customized pcDNA3.1(-) vector.

### Electrophysiology

The cDNAs for WT or mutant Dr-VSP were cotransfected with Kir2.1, KCNQ2/3, or TRPC6 into HEK293T cells using PEI Max (Polysciences, Inc.) or SuperFect (Qiagen), and Opti-MEM (Invitrogen). The cells were cultured for 6 h in Dulbecco's modified Eagle's medium (Invitrogen) supplemented with 10% FBS (GIBCO BRL) after mixing with transfection reagent. The medium was then refreshed. Electrophysiological recordings were performed 2–8 h after reseeding the transfected cells onto poly-L-lysine-coated glass-bottom dishes or coverslips (Matsunami Glass Ind.), which corresponds to 18–24 h after transfection. For recording, a dish containing HEK293T cells was placed on the stage of an inverted fluorescence microscope (IX72 or IX73, Olympus), and cells showing the fluorescence signal from EGFP (pIRES2-EGFP) or Dr-VSP<sup>mCherry</sup> were recorded. Macroscopic currents were recorded in either the whole-cell clamp or on-cell patch clamp configuration using an Axopatch-200B amplifier (Molecular Devices) or EPC800USB (HEKA).

To measure macroscopic Kir2.1 currents in the on-cell patch clamp configuration, the bath solution contained 100 mM KCl, 1 mM MgCl<sub>2</sub>, 1 mM CaCl<sub>2</sub>, and 20 mM HEPES, pH 7.2, while the pipette solution contained 10 mM KCl, 90 mM NaCl, 3 mM MgCl<sub>2</sub>, 1 mM EGTA, and 20 mM HEPES, pH 7.2. To record Kir2.1 or KCNQ2/3 currents in the whole-cell mode, the bath solution contained 10 mM KCl, 90 mM NaCl, 1 mM MgCl<sub>2</sub>, 1 mM CaCl<sub>2</sub>, and 20 mM HEPES, pH 7.2, while the pipette solution contained 100 mM KCl, 3 mM MgCl<sub>2</sub>, 1 mM EGTA, 2 mM ATP-Na<sub>2</sub>, and 20 mM HEPES, pH 7.2. A stock solution of 100 mM ATP-Na<sub>2</sub> in 20 mM HEPES was mixed with the pipette solution before use. To measure sensing currents, we used solution containing 100 mM NMDG, 3 mM MgCl<sub>2</sub>, 1 mM EGTA, and 180 mM HEPES, pH 7.0, on both sides of the cell membrane.

To measure TRPC6 currents, the standard external solution contained 140 mM NaCl, 5 mM KCl, 1 mM CaCl<sub>2</sub>, 1.2 mM MgCl<sub>2</sub>, 10 mM HEPES, and ~10 mM glucose (pH 7.4, adjusted with Tris

base; 300 mOsm, adjusted with glucose) and was always perfused. The pipette solution contained 120 mM Cs aspartate, 20 mM CsCl, 2 mM MgCl<sub>2</sub>, 5 mM EGTA, 1.5 mM CaCl<sub>2</sub>, 10 mM HEPES, 2 mM ATP-Na<sub>2</sub>, 0.1 mM GTP, and ~10 mM glucose (pH 7.2, adjusted with Tris base; 290–295 mOsm, adjusted with glucose). The diacylglycerol analogue 1-oleoyl-2-acetyl-sn-glycerol (OAG; Sigma-Aldrich), which is a TRPC6 activator, was diluted in the standard external solution from its stock concentration (50 mM in DMSO). TRPC6 currents were activated by perfusion of OAG. They reached the maximum amplitude in ~30 s after application of OAG, and then the amplitude gradually decreased for several minutes (Itsuki et al., 2012). To verify monovalent cationic currents, the external solution was replaced with NMDG solution (150 mM NMDG chloride, 10 mM HEPES, and 1 mM CaCl<sub>2</sub>, pH 7.4, adjusted with HCl) at the end of each stimulus. Stimulation, data acquisition, and analysis were performed on a computer using a Digidata 1200, 1440A, or 1550B AD/DA converter and pClamp 9.0, 10.3, or 10.7 (Molecular Devices). The pipette resistance in the solution was 2–3 MΩ for measuring ionic currents or 7–12 MΩ for measuring sensing currents. The recorded currents were low-pass filtered at 5 kHz using a four-pole Bessel filter circuit built into the amplifier, and the sampling frequency was 10–20 kHz. Current traces were digitally filtered at 1 kHz. All recordings were made at room temperature (22–26°C).

#### Simultaneous image acquisition and patch clamp

Cell imaging was performed using an electron multiplying charge-coupled device camera (ImageM C9100-13, Hamamatsu Photonics) mounted on an inverted epifluorescence microscope equipped with a 60× oil immersion objective lens (Plan ApoN, Olympus), a stable xenon lamp (U-LH75XEAP0, Olympus), and a filter set that included a BP542 (excitation filter), BP620 (emission filter), and DM570 (dichroic mirror; Olympus) along with the patch clamp setup. Image acquisition was controlled by a computer using MetaMorph (Molecular Devices). We obtained phase contrast (exposure time, 100 ms) and fluorescence images (exposure time, 1,000 ms) just before the final approach of the glass pipette to a target cell. All phase contrast images included the target cell and pipette edge (data not shown).

#### Analysis of fluorescence intensity

We used ImageJ software (National Institutes of Health) to quantify the fluorescence intensity of Dr-VSP<sup>mCh</sup> in images acquired as described above. We first calculated the average intensity of whole cell area from the obtained images. We then drew an arbitrary line on the cell, and the fluorescence intensities along the line were measured and plotted on a graph, which enabled us to determine the peak intensity at the cell contour (Fig. 4). Background fluorescence intensities were subtracted based on the average fluorescence intensity in the void area.

#### Confocal imaging

Confocal imaging was performed using the confocal microscope (LSM710, Carl Zeiss) equipped with 63× oil immersion objective lens (with numerical aperture 1.2, Carl Zeiss). The sample was

excited with the 561-nm laser and the signal was detected using a 575–610-nm bandpass filter. Image acquisition was controlled by a computer using ZEN (Carl Zeiss). An image was obtained from a single focal plane.

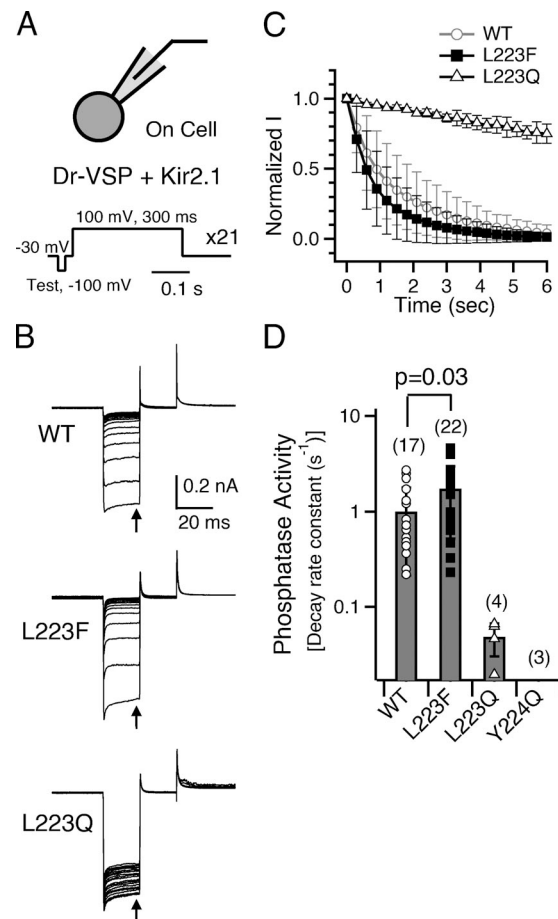


**Figure 1. Voltage-dependent phosphatase activity of WT and hydrophobic spine mutants of Dr-VSP as estimated from Kir2.1 currents.** (A) Schematic view of the protocol used to estimate VSP enzyme activity in the cell-attached patch configuration. The pulse protocol (bottom panel) consisted of a 20-ms step pulse to  $-100$  mV (test pulse to measure Kir2.1 current), followed by a 300-ms depolarization pulse to  $100$  mV (to induce VSP enzyme activity). This protocol was repeated 21 times without an interval. The holding potential was  $-30$  mV. (B) Representative Kir2.1 current traces recorded from HEK293T cells coexpressing Dr-VSP WT, L223F, or L223Q. All current traces recorded during the 21 repeated stimuli are superimposed during the first 100 ms of the pulse protocol. Inward Kir currents were elicited in hyperpolarizing test pulses, and the current amplitude gradually decreased in accordance with VSP-induced decreases in  $P(4,5)P_2$  within the plasma membrane. (C) Plots of the time-dependent changes in the normalized amplitudes of the inward Kir currents. Values were measured at the end of the 20-ms hyperpolarizing test pulses (arrows in B) and were normalized by the current amplitude during the first stimulus. Average values were connected by lines. Gray unfilled circles (WT), black squares (L223F) and black unfilled triangles (L223Q) were drawn based on data shown in B. Symbols depict the mean  $\pm$  SD of data from 17 WT, 22 L223F, or 4 L223Q cells. (D) Phosphatase activities of Dr-VSP WT and hydrophobic spine mutants (WT, L223F, L223Q, and Y224Q) estimated as rate constants for the decrease in normalized Kir currents with single exponential fitting. Fitting was applied to the dataset from each cell, then rate constants were averaged. Data are the mean  $\pm$  SD from 3 to 22 cells, and each symbol shows the data from each cell. Values in parentheses indicate the numbers of cells. Upper bars show P values from a two-tailed Student's *t* test.

**Table 1. Summary of contribution of L223F mutation and N-terminal fusion of a polypeptide from Ci-VSP to enhancement of voltage-dependent enzyme activity of eVSP**

	Phosphatase activity ( $s^{-1}$ )	Ratio	<i>n</i>	Phosphatase activity ( $s^{-1}$ )	Ratio	<i>n</i>
	Kir2.1 (on cell)			KCNQ2/3		
Dr-VSP WT	1.0 ± 0.8 <sup>a</sup>	-	17	1.6 ± 1.1 <sup>b</sup>	-	9
Dr-VSP L223F	1.7 ± 1.2 <sup>a</sup>	1.7	22	5.5 ± 4.0 <sup>b</sup>	3.4	9
	Phosphatase activity ( $s^{-1}$ )	Ratio	<i>n</i>	Phosphatase activity ( $\times 10^2$ ms)	Ratio	<i>n</i>
	Kir2.1 (whole cell)			TRPC6		
Dr-VSP <sup>mChe</sup> WT	2.6 ± 2.6 <sup>c,d,e</sup>	-	7			
Dr-VSP <sup>mChe</sup> L223F	4.6 ± 1.6 <sup>c,f</sup>	1.8	8			
CiDr-VSP <sup>mChe</sup> WT	3.6 ± 2.2 <sup>d,g</sup>	1.4	10	4.1 ± 1.7 <sup>h</sup>	-	6
CiDr-VSP <sup>mChe</sup> L223F	7.3 ± 3.0 <sup>e,f,g</sup>	2.8	11	2.0 ± 0.9 <sup>h</sup>	2.1	3

Phosphatase activity is shown as the rate constant ( $s^{-1}$ ) or time lag (ms) calculated from inward current decay of Kir2.1 or time-dependent change of TRPC6 current, respectively. Ratio is a comparison between the phosphatase activity of a target and WT. *n* is sample number. P values were calculated by two-tailed Student's *t* test.

<sup>a</sup>P = 0.03.

<sup>b</sup>P = 0.03.

<sup>c</sup>P = 0.13.

<sup>d</sup>P = 0.46.

<sup>e</sup>P = 0.005.

<sup>f</sup>P = 0.03.

<sup>g</sup>P = 0.007.

<sup>h</sup>P = 0.04.

## Data analysis

Data were analyzed using Excel (Microsoft), ImageJ or Fiji (National Institutes of Health), Clampfit (Molecular Devices), MATLAB (MathWorks), Prism (GraphPad Software), and Igor Pro (WaveMetrics) software. Data are presented as means ± SD. Statistical significance was assessed using two-tailed Student's *t* tests or two-way ANOVA.

## Results

### An aromatic ring mutation in the hydrophobic spine induces a higher enzymatic activity in Dr-VSP

Dr-VSP is better expressed in mammalian cultured cells than in *Xenopus laevis* oocytes (Hossain et al., 2008; Okamura et al., 2009). We previously reported that the voltage-dependent phosphatase activity of Ci-VSP reflects the hydrophobicity of the structure on membrane-protein interface in the phosphatase domain (Leu-284 and Phe-285), which protrudes toward the membrane. We call this structure the hydrophobic spine (Kawanabe et al., 2018). Increasing the hydrophobicity of the spine in Ci-VSP through amino acid replacement increased the voltage-dependent enzyme activity. To test whether a similar change takes place upon amino acid substitution in the corresponding region of Dr-VSP, the WT enzyme or a mutant in which Leu-223 or Tyr-224 in the hydrophobic spine was replaced with Phe or Gln were heterologously expressed in HEK293T cells. An inward rectifying K<sup>+</sup> channel (mouse Kir2.1) was used for the read out of the voltage-dependent phosphatase activity toward PI(4,5)P<sub>2</sub> in the plasma membrane, as previously established (Murata and Okamura, 2007; Sakata and Okamura, 2014; Rjasanow et al., 2015; Tang et al., 2015).

Fig. 1 shows representative current traces from cells coexpressing Dr-VSP WT or a hydrophobic spine mutant (L223F or L223Q) with Kir2.1 recorded in the on-cell patch clamp configuration. The pulse protocol was composed of two parts (Fig. 1 A): (1) a 20-ms step pulse to -100 mV to determine the steady-state Kir current amplitude (test pulse), and (2) a 300-ms depolarizing step pulse to 100 mV to activate Dr-VSP. A large Kir current was detected in the first episode during the test pulse to -100 mV (Fig. 1 B). This was followed by a gradual decrease in the Kir current amplitude with repeated stimulations. When the normalized Kir currents measured at the end of the 20-ms test pulse were plotted against the accumulated depolarization time (e.g., first, 0 ms; second, 300 ms; Fig. 1 C), the kinetics of the decrease in the Kir current reflected the voltage-dependent phosphatase activity. The rate constants of single exponential decay of Kir current were compared in Fig. 1 D. The L223F mutant produced a more rapid Kir current decrease than did WT Dr-VSP (Fig. 1, B-D; and Table 1). By contrast, L223Q, in which a hydrophilic amino acid was introduced into the hydrophobic spine, produced a slower Kir current decrease, indicating that the voltage-dependent phosphatase activity is diminished in the mutant (Fig. 1, B-D). Another hydrophilic mutant, Y224Q, was also tested, and it showed less or no phosphatase activity (Fig. 1 D). These results are consistent with an earlier report on Ci-VSP (Kawanabe et al., 2018).

VSP has also been studied with another voltage-gated K<sup>+</sup> channel, KCNQ2/3 (Kv7.2/7.3; Rjasanow et al., 2015; Hossain et al., 2008; Falkenburger et al., 2010). KCNQ2/3 binds PI(4,5)P<sub>2</sub> with weaker affinity than does Kir2.1, and the dynamic range of the sensitivity differs between the two channels (Rjasanow et al., 2015). Fig. 2 shows representative outward KCNQ2/3

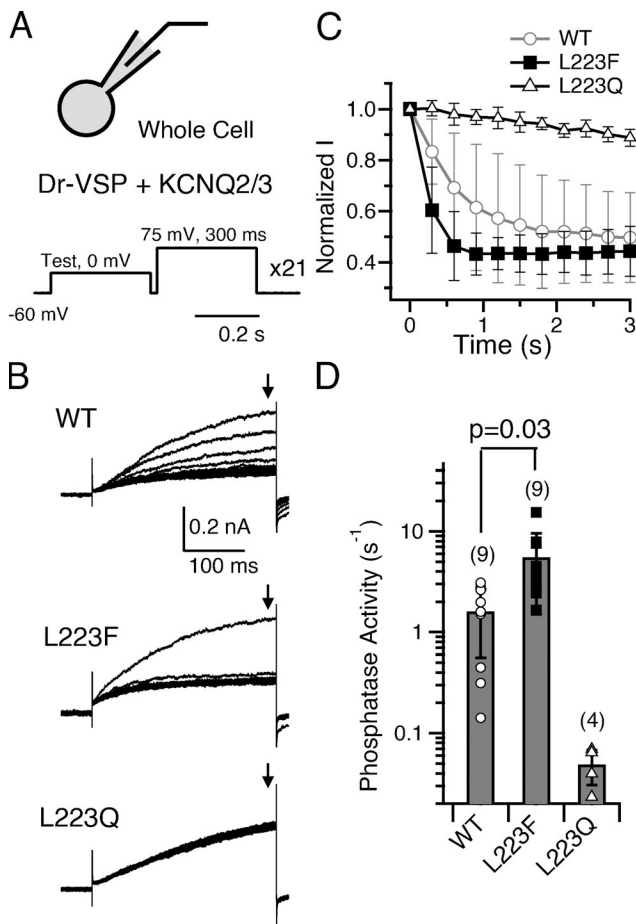


**Figure 2. Effects of mutation within the hydrophobic spine of Dr-VSP as estimated from KCNQ2/3 currents.** (A) Schematic view of the protocol for examining VSP enzyme activity in the whole-cell patch configuration. The pulse protocol used to estimate VSP activity (bottom panel) consisted of a 300-ms step pulse to 0 mV (test pulse) and a 300-ms depolarization pulse to 75 mV. This protocol was repeated 21 times without an interval. The holding potential was  $-60$  mV. (B) Representative traces of outward KCNQ2/3 currents elicited by depolarization to 0 mV in HEK293T cells coexpressing Dr-VSP WT, L223F, or L223Q. The traces of KCNQ2/3 currents elicited by the 21-times repeated stimuli are superimposed. (C) Plots of the time-dependent changes in the amplitudes of the outward KCNQ2/3 currents. Values were measured at the end of the depolarizing test pulses (arrows in B) and normalized by the current amplitude during the first stimulation. Gray unfilled circles (WT), black squares (L223F), and black unfilled triangles (L223Q) were drawn based on the data shown in B. Average values were connected by lines. Symbols depict the mean  $\pm$  SD of data from nine WT, nine L223F, or four L223Q cells. (D) Rate constants for the declines in the normalized KCNQ2/3 currents with single exponential fitting are shown as phosphatase activities of WT, L223F, and L223Q. Single exponential fitting was performed with the dataset from each cell. Data are the mean  $\pm$  SD from four to nine cells, and each symbol shows the data from each cell. Values in parentheses indicate the numbers of cells. Upper bars show P values from a two-tailed Student's t test.

current traces recorded from cells expressing Dr-VSP WT or a hydrophobic spine mutant. The pulse protocol consisted of a test pulse (0 mV, 300 ms) and a depolarization step (75 mV, 300 ms, for activating VSP; Fig. 2A). A slowly activating outward current was observed in the first trace during a test pulse to 0 mV, and the current amplitudes decreased in the subsequent traces with

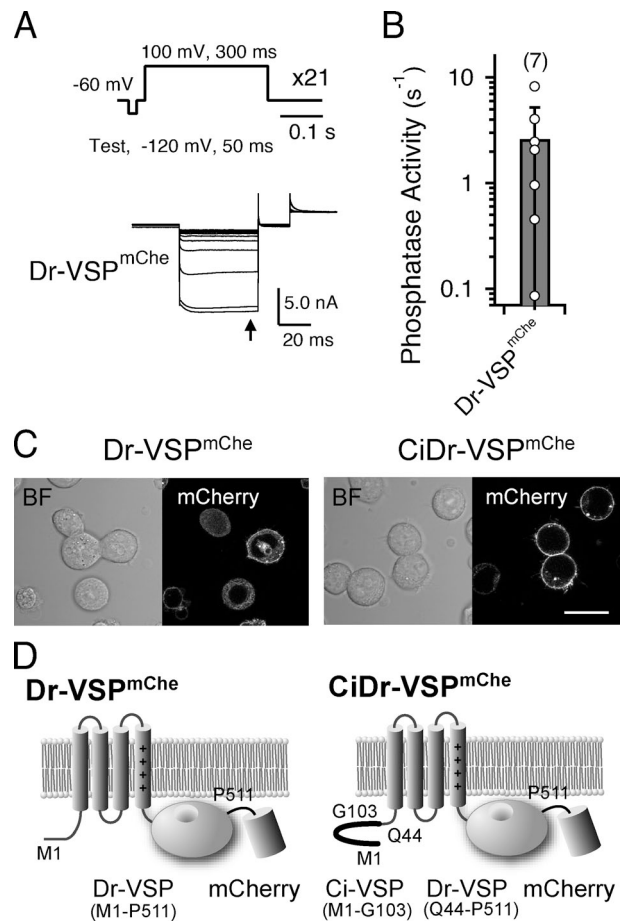


**Figure 3. Membrane localization of Dr-VSP.** (A) Representative current traces of Kir2.1 recorded from HEK293T cells coexpressed with mCherry fused Dr-VSP WT in pcDNA3.1 (lower) with whole-cell patch configuration. The pulse protocol used to estimate VSP activity (upper) consisted of a 50-ms step pulse to  $-120$  mV (test pulse) and a 300-ms depolarization pulse to 100 mV. This protocol was repeated 21 times without an interval. The holding potential was  $-60$  mV. (B) The phosphatase activities of Dr-VSP<sup>mCherry</sup>. Data are the mean  $\pm$  SD from seven cells, and each symbol shows the data from each cell. Two cells showed no phosphatase activity and were excluded from the analysis. Values in parentheses indicate the numbers of cells. (C) Representative confocal microscope images of Dr-VSP<sup>mCherry</sup> (left) and a chimeric protein (Ci-VSP [M1-G103] + Dr-VSP [Q44-P511] [CiDr-VSP<sup>mCherry</sup>]; right) expressed in HEK293T cells. Bright field images (BF) and fluorescence images of mCherry are shown. Scale bar, 20  $\mu$ m. (D) Topologies of Dr-VSP<sup>mCherry</sup> (left) and CiDr-VSP<sup>mCherry</sup> (right).

all three constructs (Dr-VSP WT, L223F, and L223Q). When the time constants for the decrease in KCNQ2/3 currents were estimated by fitting with a single exponential function, L223F induced a faster decrease in the KCNQ2/3 current than did WT Dr-VSP (Fig. 2, B-D; and Table 1). On the other hand, the current decrease exhibited slower kinetics in cells expressing L223Q (Fig. 2, B-D). These results are consistent with those obtained using Kir2.1 as the PI(4,5)P<sub>2</sub> reporter.

#### Improvement of cell surface localization

We have shown that Dr-VSP with a Phe mutation within the hydrophobic spine has higher voltage-dependent phosphatase activity than the WT enzyme. However, the apparent enzymatic

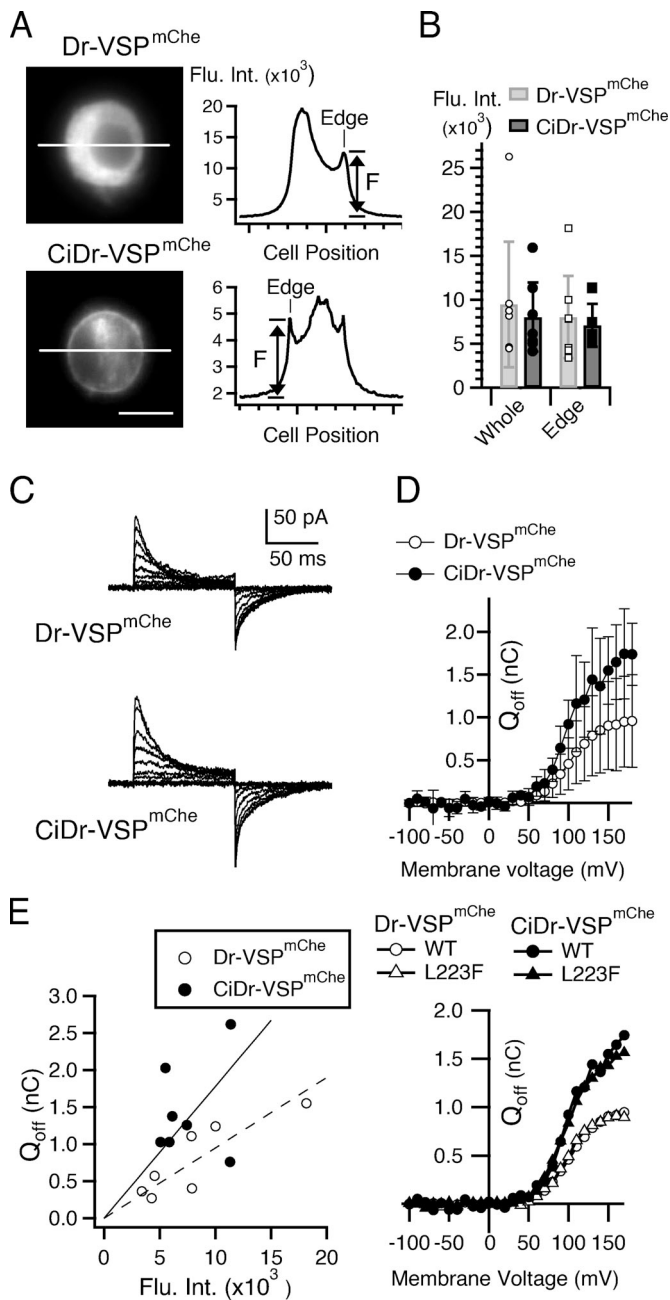


**Figure 4. N-terminal region of Ci-VSP enhanced membrane targeting of Dr-VSP.** (A) Representative fluorescence images of cells expressing Dr-VSP<sup>mCh</sup> (upper) or CiDr-VSP<sup>mCh</sup> (lower). Fluorescence intensities along the lines drawn through cells are shown in the right graph. Edge in the kymograph indicates the cell contour, and its fluorescence intensity was indicated by "F." Scale bar, 10  $\mu$ m. (B) Average fluorescence intensity over the whole cell area and the peak intensity in cell contour (edge) estimated from images of Dr-VSP<sup>mCh</sup> and CiDr-VSP<sup>mCh</sup> fluorescence. Data are the mean  $\pm$  SD from seven cells and each symbol shows the data from one cell. (C) Representative traces of sensing current that were measured using the solution specific for sensing current measurement. The currents were measured by applying depolarizing step pulses (-100 mV to 170 mV in 10-mV increments) from the holding potential (-60 mV) with the P/-4 method, though the traces shown are in 20-mV increments. (D) Top: Q-V relationships of Dr-VSP<sup>mCh</sup> and CiDr-VSP<sup>mCh</sup>. The charge movements in the repolarization step (Q<sub>off</sub>) were estimated by integration of the Q<sub>off</sub>. Unfilled and filled circles represent Dr-VSP<sup>mCh</sup> and CiDr-VSP<sup>mCh</sup>, respectively. Error bars indicate the SD (Dr-VSP<sup>mCh</sup>: n = 7 [-100 to ~170 mV], CiDr-VSP<sup>mCh</sup>: n = 7, 6, 4, 3 [-100

activity of VSP will also depend on the level of its surface expression (Murata and Okamura, 2007). In *Xenopus* oocytes, the expression level can be controlled by regulating the amount of injected RNA (Rayaprolu et al., 2018). On the other hand, the protein expression level in transfected cultured cells often varies from cell to cell dependent on the copy number of introduced plasmids.

Therefore, we detected the cell surface fluorescence signal from a fluorescent protein (mCherry) fused to Dr-VSP (Dr-VSP<sup>mCh</sup>). After transfection into HEK293T cells, we verified the voltage-dependent phosphatase activity of Dr-VSP<sup>mCh</sup> by measuring the time course of the decrease in Kir2.1 currents by whole-cell patch recording (Fig. 3 A), indicating that fusion of mCherry does not affect the intrinsic phosphatase activity of Dr-VSP.

We noticed that the phosphatase activities in Dr-VSP<sup>mCh</sup> showed a large variance and cells with bright fluorescence often showed little or no phosphatase activity, as detected through activation of coexpressed K<sup>+</sup> channels. We suspect that overexpression of Dr-VSP<sup>mCh</sup> may have had a toxic effect on these cells, possibly due to mistargeting of the overexpressed Dr-VSP<sup>mCh</sup> to intracellular compartments. Confocal microscopic examination showed that the fluorescence signal from Dr-VSP<sup>mCh</sup> not only was present at the cell surface but was also widely distributed throughout the intracellular compartments (Fig. 3 C, left, mCherry).

To facilitate cell surface expression, the N-terminal cytoplasmic region of Ci-VSP (M1-G103), which is known to facilitate the enzyme's membrane targeting (Tsutsui et al., 2013), was fused to the main body of Dr-VSP (Q44-P511; Fig. 3 D). Most cells transfected with this chimeric protein exhibited a more discrete distribution that most likely corresponded to the plasma membrane, suggesting CiDr-VSP<sup>mCh</sup> is more selectively localized to the cell membrane than Dr-VSP<sup>mCh</sup> (Fig. 3 C).

To confirm whether this chimeric version of Dr-VSP harboring the N-terminal region of Ci-VSP is more highly localized to the plasma membrane than Dr-VSP, we compared the fluorescence intensity and the sensing charge from the same cells. Sensing (or gating) charges are known to provide a reliable quantitative estimate of functional voltage-gated ion channels on cell membranes (Hille, 2001) and VSP (Murata and Okamura, 2007). We first acquired a fluorescence image of Dr-VSP<sup>mCh</sup>-expressing cells using an electron multiplying charge-coupled device camera mounted on an epifluorescence microscope

to ~130, 140, 150, and 160 to ~170 mV]). Datasets of Dr-VSP<sup>mCh</sup> and CiDr-VSP<sup>mCh</sup> (70 to ~130 mV) were compared with repeated-measures two-way ANOVA. There was a significant difference between these two groups (P = 0.05). Bottom: Q-V relationships of Dr-VSP<sup>mCh</sup> WT, L223F, CiDr-VSP<sup>mCh</sup> WT, and L223F (Dr-VSP<sup>mCh</sup> WT and CiDr-VSP<sup>mCh</sup> WT are equal to Dr-VSP<sup>mCh</sup> and CiDr-VSP<sup>mCh</sup> in other panels, respectively). Error bars were not shown to make averaged values easier to see. Parameters of these Q-V curves were shown in Table 1. (E) Relationship between the Q<sub>off</sub> and the fluorescence intensity in the cell contour. In this Q<sub>off</sub>, we chose the value of Q<sub>off</sub> measured at the holding potential after depolarizing at 130 mV, since recordings at more than 140 mV were often unsuccessful due to unstable cell membrane. Each point shows a value from one cell and fitted by linear function (slope, 1.78  $\times 10^{-4}$  in Dr-VSP<sup>mCh</sup>; 0.95  $\times 10^{-4}$  in CiDr-VSP<sup>mCh</sup>).

Table 2. Fitting parameter of Q-V relationships

	$V_{1/2}$ (mV)	Z	A (nC)	n
Dr-VSP <sup>mChe</sup> WT	103 ± 5 <sup>a,b,c</sup>	1.4 ± 0.1 <sup>d,e,f</sup>	1.1 ± 0.6 <sup>g,i</sup>	6
Dr-VSP <sup>mChe</sup> L223F	96 ± 4 <sup>a</sup>	1.7 ± 0.1 <sup>d</sup>	1.1 ± 0.3 <sup>h,i</sup>	4
CiDr-VSP <sup>mChe</sup> WT	98 ± 4 <sup>b</sup>	1.4 ± 0.2 <sup>e</sup>	1.6 ± 0.4 <sup>g,i</sup>	4
CiDr-VSP <sup>mChe</sup> L223F	96 ± 5 <sup>c</sup>	1.4 ± 0.1 <sup>f</sup>	1.6 ± 0.6 <sup>h,i</sup>	6

Q-V curves shown in Fig. 4 D were fitted by single Boltzman distribution,  $Q(V) = A\{1 + \exp[(V - V_{1/2})/\text{slope}]\}$ , where “A” is the maximum charge amplitude, “V” is the membrane potential for test pulse, “ $V_{1/2}$ ” is the half-maximum membrane potential, and “slope” is the steepness of the curve in mV per e-fold change. The effective valence, “Z” is calculated by  $\text{slope} = k_B T / Ze$ , where the parameter “e” is elementary electric charge, “ $k_B$ ” is Boltzmann constant, and “T” is the absolute temperature. All data are shown as mean ± SD. n is the sample number. The statistical significance of differences was evaluated by a two-tailed Student’s t test. Sample numbers are different from those of Fig. 4, because fitting parameters in the table were obtained only from a set of cells that were able to be recorded over 150 mV.

<sup>a</sup>P = 0.08.

<sup>b</sup>P = 0.25.

<sup>c</sup>P = 0.06.

<sup>d</sup>P = 0.02.

<sup>e</sup>P = 0.93.

<sup>f</sup>P = 0.54.

<sup>g</sup>P = 0.13.

<sup>h</sup>P = 0.13.

<sup>i</sup>P = 0.03 (Dr-VSP<sup>mChe</sup> vs. CiDr-VSP<sup>mChe</sup>).

within the patch clamp setup, and then made whole-cell recordings to measure the sensing currents. As shown in the representative images of Dr-VSP<sup>mChe</sup> and CiDr-VSP<sup>mChe</sup> (Fig. 4 A), we evaluated two signals in the fluorescence images: the average intensity over the whole cell area and the intensity at the cell contour (Fig. 4 B). The fluorescence intensity at the contour was estimated by measuring the peak intensity at the cell “edge” along a white line on cell fluorescence images (Fig. 4 A). We detected no difference of the fluorescence magnitude over the whole cell area or cell contour between Dr-VSP<sup>mChe</sup> and CiDr-VSP<sup>mChe</sup> (Fig. 4 B).

Dr-VSP sensing currents were measured in whole-cell patch recordings with the NMDG-based intracellular and extracellular solution appropriate for sensing currents (Fig. 4 C). The off-sensing charges (Q<sub>off</sub>) were calculated by integrating the sensing currents upon repolarization step and plotted against the depolarized membrane voltage of test pulse (charge-voltage [Q-V] relationship; Fig. 4 D). CiDr-VSP<sup>mChe</sup> exhibited greater Q<sub>off</sub> than Dr-VSP<sup>mChe</sup> with no significant change of its voltage dependency (Table 2), which suggests that CiDr-VSP<sup>mChe</sup> is more localized to the plasma membrane than Dr-VSP<sup>mChe</sup>. Q-V curves showed that the magnitude of the Q<sub>off</sub> significantly differs between Dr-VSP<sup>mChe</sup> and CiDr-VSP<sup>mChe</sup> (P = 0.05 by repeated-measures two-way ANOVA; see Fig. 4 D legend for details). Q-V relationships of four constructs (Dr-VSP<sup>mChe</sup> WT, L223F and CiDr-VSP<sup>mChe</sup> WT, L223F) are shown in Fig. 4 D (lower panel). Magnitudes of Q<sub>off</sub> in Dr-VSP<sup>mChe</sup> L223F and CiDr-VSP<sup>mChe</sup> L223F show similar difference as in the WT pair, verifying that fusion of the N-terminal region of Ci-VSP to Dr-VSP enhances

cell surface expression. In either case, with or without N-terminal Ci-VSP sequence, the Q<sub>off</sub> curves for WT and L223F were superimposed on each other, suggesting that voltage dependence was not significantly altered by mutation in the hydrophobic spine (Table 2).

A plot of the fluorescence intensity of mCherry in the cell contour against Q<sub>off</sub> (charge-fluorescence [Q-F] relationship; Fig. 4 E) shows that the linear relationship between Q<sub>off</sub> and fluorescence is steeper for CiDr-VSP<sup>mChe</sup> than for Dr-VSP<sup>mChe</sup> (slope,  $1.78 \times 10^{-4}$  in Dr-VSP<sup>mChe</sup>;  $0.95 \times 10^{-4}$  in CiDr-VSP<sup>mChe</sup>), suggesting that the Dr-VSP<sup>mChe</sup> fluorescence of the cell contour (Fig. 4, A and B) estimated based on epifluorescence microscopy includes any signal beneath the cell membrane. Q<sub>off</sub> was measured at the holding potential after depolarizing to 130 mV, where the magnitude of sensing charge does not attain a saturated level, since we could not obtain the data due to unstable membrane at the higher voltage. Thus, detection of cell surface expression level of Dr-VSP<sup>mChe</sup> by epifluorescence microscopy provides a less reliable estimate than quantification by measuring sensing current. Most importantly, these results are consistent with the idea of more selective cell membrane localization of CiDr-VSP<sup>mChe</sup> than in Dr-VSP<sup>mChe</sup>.

#### eVSP

The L223F mutation within the hydrophobic spine of Dr-VSP enhanced its phosphatase activity. In addition, creation of the CiDr-VSP<sup>mChe</sup> chimera enhanced its selective accumulation in the cell membrane. These two features were combined in CiDr-VSP<sup>mChe</sup> L223F (eVSP). The enzyme activity of CiDr-VSP<sup>mChe</sup> L223F (eVSP) was examined using Kir2.1 channel currents as the readout. Fig. 5 shows a comparison of the voltage-dependent enzyme activity among four versions, Dr-VSP<sup>mChe</sup> WT, Dr-VSP<sup>mChe</sup> L223F, CiDr-VSP<sup>mChe</sup> WT, and CiDr-VSP<sup>mChe</sup> L223F (eVSP), as reflected by the Kir2.1 channel activity (Fig. 5 A).

Among the four constructs, CiDr-VSP<sup>mChe</sup> L223F (eVSP) mediated the most rapid current decrease when these were examined with repeated depolarizing pulses to 100 mV (Fig. 5, A-C; and Table 1). CiDr-VSP<sup>mChe</sup> WT showed similar phosphatase activity of the Dr-VSP<sup>mChe</sup> WT (P = 0.46). However, when the phosphatase activity of both constructs was measured at 75 mV (Fig. 5 D), CiDr-VSP<sup>mChe</sup> WT ( $1.8 \pm 1.6 \text{ s}^{-1}$ ) showed slightly higher activity than Dr-VSP<sup>mChe</sup> WT ( $0.6 \pm 1.0 \text{ s}^{-1}$ , P = 0.10). CiDr-VSP<sup>mChe</sup> L223F (eVSP) showed significantly higher phosphatase activity than Dr-VSP<sup>mChe</sup> L223F (P = 0.03; Fig. 5 C). These results support the idea that increase of cell surface expression by the addition of the N-terminal region of Ci-VSP contributed to increase of the activity of voltage-dependent enzyme. On the other hand, there is also increase in phosphatase activity measured at 75 or 100 mV from Dr-VSP<sup>mChe</sup> WT to L223F mutant (P = 0.01 or 0.13), and from CiDr-VSP<sup>mChe</sup> WT to its L223F mutant (eVSP; P = 0.03 or 0.007; Fig. 5 C). We also performed two control experiments with CiDr-VSP<sup>mChe</sup> L223F/C302S (C302S is a defective mutation of Dr-VSP’s enzyme activity; Hossain et al., 2008) or Kir2.1 alone. Both showed no current decay during application of the same pulse protocol of other constructs (Fig. 5, A-C). Measurements at different depolarizing membrane potentials (Fig. 5 D) showed that the four

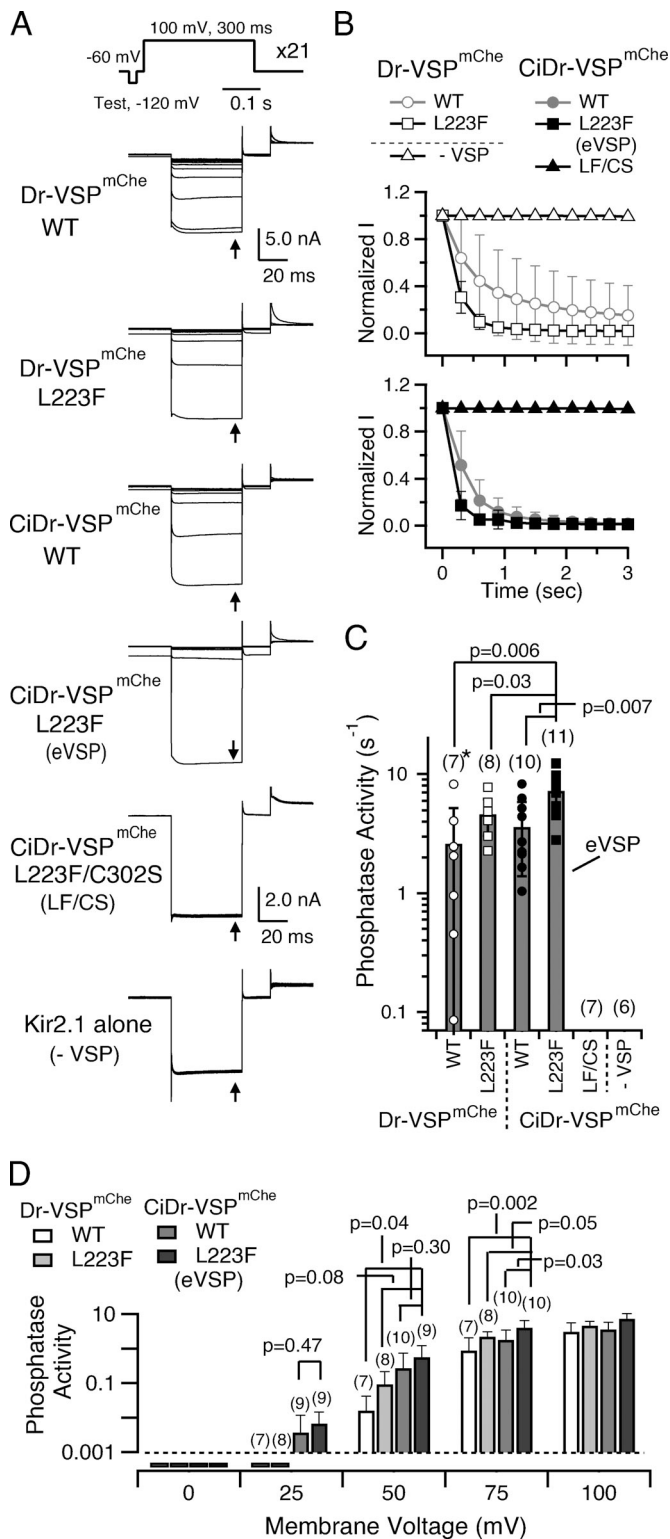


**Figure 5. eVSP CiDr-VSP<sup>mChe</sup> L223F.** (A) Representative Kir2.1 current traces recorded from HEK293T cells coexpressing Dr-VSP<sup>mChe</sup> WT, Dr-VSP<sup>mChe</sup> L223F, CiDr-VSP<sup>mChe</sup> WT, CiDr-VSP<sup>mChe</sup> L223F (eVSP), CiDr-VSP<sup>mChe</sup> L223F/C302S (eVSP with activity-null mutation: LF/CS), and Kir2.1 alone (-VSP). Holding potential was set to -60 mV and depolarizing step for activating VSP was repeatedly applied (21 times) to 100 mV for 300 ms (the protocol shown at the top). All 21 traces were superimposed in each panel. (B) Time-dependent changes in the normalized amplitudes of Kir2.1 currents in cells coexpressing Dr-VSP<sup>mChe</sup> WT (unfilled gray circles), Dr-VSP<sup>mChe</sup> L223F

active constructs produced more rapid decay of Kir2.1 channel currents as the depolarizing membrane potential becomes higher (Fig. 5 D) and that decay kinetics seem almost saturated at 100 mV in each construct. Fold increases of voltage-dependent enzyme activity estimated by the Kir2.1 channel activities among different constructs (Table 1) indicate that facilitation of selective cell surface expression as well as mutation of L223F both contributed to enhancement of the activity of voltage-dependent decrease of PI(4,5)P<sub>2</sub> by eVSP.

We tried to validate the usefulness of eVSP as a tool using TRPC6, which is also sensitive to PI(4,5)P<sub>2</sub> (Imai et al., 2012; Itsuki et al., 2012). In contrast to Kir2.1, with TRPC6, the readout channel activity can be monitored during a single long depolarizing pulse that simultaneously activates the channel and VSP, thereby making repetition of depolarizing pulses for stimulation of VSP unnecessary. The traces in Fig. 6 show representative outward and inward Ca<sup>2+</sup> currents through TRPC6 with CiDr-VSP<sup>mChe</sup> WT and L223F (eVSP) in the presence of the TRPC6 activator OAG. A test pulse was stepped to 100 mV (Fig. 6 A). At the holding potential of -50 mV, small stable inward TRPC6 currents were observed, which were not present in the absence of OAG. During depolarization, large outward currents were observed. Then, a gradual current decrease was observed with CiDr-VSP<sup>mChe</sup> WT, whereas a more rapid current decrease was observed with CiDr-VSP<sup>mChe</sup> L223F (eVSP; Fig. 6 B), indicating that PI(4,5)P<sub>2</sub> depletion by eVSP is faster. We estimated “time lag” between the onset of the depolarization (+100 mV) and the onset of the current suppression (cross points of dotted lines), which reflects the phosphatase activity (Fig. 6, C and D; and Table 1). Upon repolarization, gradual current recovery was observed. Although recovery rates seemed to be different between the two constructs in traces of B, there was no statistical difference (time constant of recovery phase: CiDr-VSP<sup>mChe</sup> WT, 2.6  $\pm$  0.4 s [*n* = 6]; CiDr-VSP<sup>mChe</sup> L223F [eVSP], 3.2  $\pm$  0.6 s [*n* = 3], *P* = 0.58 by two-tailed Student's *t* test). Cells coexpressing TRPC6 with the enzyme-defective mutant, C302S, of Dr-VSP (Hossain et al., 2008) did not exhibit depolarization-induced current decline (Fig. 6 B, bottom).

(unfilled black squares), CiDr-VSP<sup>mChe</sup> WT (filled gray circles), CiDr-VSP<sup>mChe</sup> L223F (filled black squares), CiDr-VSP<sup>mChe</sup> L223F/C302S (LF/CS, unfilled gray triangles), or Kir2.1 alone (-VSP, unfilled black triangles) with repeated depolarizing pulses to 100 mV. Amplitudes of Kir2.1 currents were measured at the end of the hyperpolarizing test pulses (-120 mV, 50 ms; arrows in A). Values were normalized by the current amplitude during the first test pulse. Symbols depict the mean  $\pm$  SD from 6 to 11 cells. (C) Phosphatase activities of Dr-VSP<sup>mChe</sup> WT, Dr-VSP<sup>mChe</sup> L223F, CiDr-VSP<sup>mChe</sup> WT, CiDr-VSP<sup>mChe</sup> L223F (eVSP), CiDr-VSP<sup>mChe</sup> L223F/C302S (LF/CS), and Kir2.1 alone (-VSP). Rate constants for the declines in normalized Kir2.1 currents with single exponential fitting are shown as phosphatase activities. The values of the mean  $\pm$  SD and individual plots are shown. Two cells expressing Dr-VSP<sup>mChe</sup> WT showed no phosphatase activity and were excluded from these data (\*). Values in parentheses indicate the numbers of cells. Upper bars show P values from a two-tailed Student's *t* test. (D) Phosphatase activities estimated by different depolarizing conditions. White, light gray, dark gray, and dim gray bars show Dr-VSP<sup>mChe</sup> WT, Dr-VSP<sup>mChe</sup> L223F, CiDr-VSP<sup>mChe</sup> WT, and CiDr-VSP<sup>mChe</sup> L223F, respectively. Horizontal axis shows the depolarizing voltage condition: 0, 25, 50, 75, and 100 mV. The data in 100 mV are the same data as those shown in C.

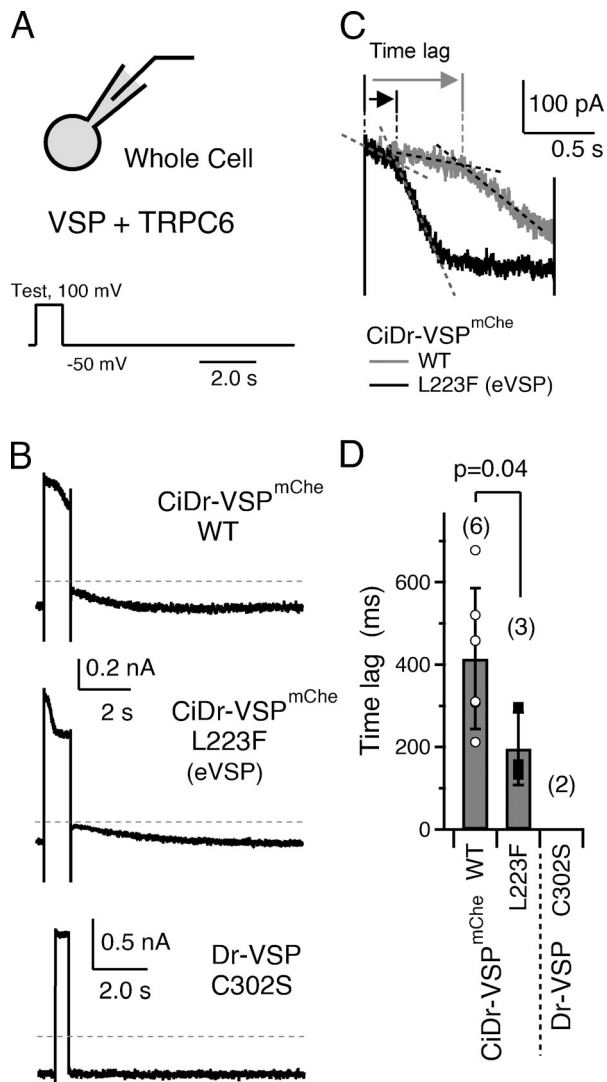


**Figure 6. Application of eVSP to TRPC6.** (A) Schematic view of the protocol used to test the PI(4,5)P<sub>2</sub> sensitivity of TRPC6 using VSP in the whole-cell patch configuration. The bath solution was always perfused, and OAG, a TRPC6 activator, was added just before measurement. While TRPC6 channel is activated by OAG (see Materials and methods for details), we repeatedly tested TRPC6 current with VSP by depolarization pulse as shown in the bottom panel. A single 500- or 1,000-ms depolarizing pulse was stepped to 100 mV. The holding potential was -50 mV. (B) Representative TRPC6 current traces recorded from HEK293T cells coexpressing CiDr-VSP<sup>mChe</sup> WT (upper), L223F (middle, eVSP), or Dr-VSP C302S (lower). Dashed lines indicate 0 level. (C) Enlarged and superimposed view of current traces during the depolarizing test pulse shown in B. The gray and black lines show CiDr-VSP<sup>mChe</sup> WT and CiDr-VSP<sup>mChe</sup> L223F (eVSP), respectively. The scale bar refers commonly to the TRPC6 current waveform with CiDr-VSP<sup>mChe</sup> WT (gray line) and the TRPC6 current waveform with CiDr-VSP<sup>mChe</sup> L223F (black line). Arrows indicate the time lag between the onset of the depolarization (+100 mV) and the onset of the current suppression (cross points of two dotted lines). Traces are superimposed from B by y axis offset without a scale change. (D) Plots of the time lag of three constructs. Data are the mean ± SD from two to six cells, and each symbol shows the data from each cell. Values in parentheses indicate the numbers of cells. In the case of Dr-VSP C302S, the time lag was not calculated because of no current decay. Upper bars show P values from a two-tailed Student's *t* test.

## Discussion

We have been able to enhance the activity of Dr-VSP by modifying the protein in two ways. The voltage-dependent phosphatase activity of Dr-VSP was enhanced by introducing an aromatic residue at the position of Leu-223 within the hydrophobic spine, a membrane-interacting region of the phosphatase domain. In addition, selective plasma membrane targeting of Dr-VSP was enhanced by fusion with the N-terminal region of Ci-VSP, which was previously shown to facilitate cell surface expression. The increased enzymatic activity of this modified version of Dr-VSP (CiDr-VSP<sup>mChe</sup> L223F, eVSP) was verified based on the activities of coexpressed Kir2.1 and TRPC6 channels.

We assume that eVSP will serve as a better tool than the plain Dr-VSP based on two factors: better selective cell surface expression and higher phosphatase activity. eVSP showed an ~2.8-fold increase of phosphatase activity over Dr-VSP as examined at 100 mV using the Kir2.1 as the readout (Fig. 5 C and Table 1). We were unable to determine how cell surface expression correlated with increase of phosphatase activity in HEK293T cells, since sensing charges and phosphatase activity were not able to be analyzed in the same cells in our experimental setup. Our trial of quantification of cell surface expression of Dr-VSP<sup>mChe</sup> and its mutant by epifluorescence microscope was unsuccessful, since signals beneath the cell membrane were not completely separated. It is unlikely that apparent increase of voltage-dependent phosphatase activity of L223F mutation is through facilitated cell surface expression for two reasons. First, values of sensing charge, representing the number of cell surface VSP molecules, were not significantly different between eVSP and CiDr-VSP<sup>mChe</sup> WT (Fig. 4). In addition, our previous study (Kawanabe et al., 2018) showed that Ci-VSP L284F, the construct with mutation of hydrophobic spine which corresponds to L223F mutation of Dr-VSP, did not show significant difference in cell surface expression from that of Ci-VSP WT. In the paper, detailed analysis of motions both of the VSD and the cytoplasmic enzyme region led to the conclusion that both phosphatase activity and coupling efficiency were facilitated in Ci-VSP L284F without showing a shift of voltage dependence of VSD motion. In the present study as well, sensing charges exhibited similar voltage dependence among the WT and L223F mutant (Table 2). Voltage dependence of enzyme activity of VSP is dictated by that of the VSD as long as the VSD is tightly coupled with the enzyme region (Sakata et al., 2011; Sakata and Okamura, 2014). Therefore, we assume that eVSP has higher maximum enzyme activity per molecule than WT Dr-VSP without shift of the voltage-enzyme relationship. More rigorous quantitative analysis such as analysis of raw results using the mathematical models (Sakata et al., 2011; Keum et al., 2016) may help to clarify in more detail how properties of eVSP are distinct from those of WT.

Many ion channels and transporters have been shown to be sensitive to PIs (Suh and Hille, 2005; Hille et al., 2015; Okamura et al., 2018). However, in cases where the binding affinity between the ion channel and PI is very high, the functional significance of the PI-channel interaction may be unknown. For example, the recently solved protein structure of the  $\gamma$ -aminobutyric acid A (GABA<sub>A</sub>) receptor contains two

molecules of PI(4,5)P<sub>2</sub> within the single channel complex (Laverty et al., 2019), but the functional significance of this PI(4,5)P<sub>2</sub> binding has yet to be determined (Mennerick et al., 2014), possibly due to the very high binding affinity and the inability to experimentally induce release of the PI(4,5)P<sub>2</sub> from the channel complex.

CiDr-VSP<sup>mChe</sup> L223F (eVSP) could potentially serve as a useful tool in future studies of the function of PI(4,5)P<sub>2</sub> tightly bound to ion channels in heterologous mammalian cells. Experiments with various cell lines and primary cultures (e.g., muscle cells or neurons) will be necessary to further evaluate the usefulness of eVSP. In addition, VSP shows enzyme activity not only toward PI(4,5)P<sub>2</sub> but also for PI(3,4,5)P<sub>3</sub> and PI(3,4)P<sub>2</sub>. Whether enzyme activity for PI(3,4,5)P<sub>3</sub> or PI(3,4)P<sub>2</sub> is also enhanced in eVSP remains an important question to be addressed in the future. Finally, we anticipate that further remodeling based on the molecular mechanisms of VSP will lead to further improvements in the properties of VSP for use as a molecular tool.

## Acknowledgments

David A. Eisner served as editor.

We thank Dr. Yoshihiro Kubo for providing Kir2.1 plasmid, Dr. Bertil Hille for providing KCNQ2-YFP and KCNQ3-YFP plasmids, and Drs. Thomas Hofmann and Michael Schaefer for providing human TRPC6 plasmid. We also thank Dr. Yasuo Mori for encouragement and the Center for Medical Research and Education, Graduate School of Medicine, Osaka University for technical support.

This work was supported by Ministry of Education, Culture, Sports, Science and Technology Japan/Japan Society for the Promotion of Science KAKENHI grant nos. JP25253016 (Y. Okamura), JP15H05901 (Y. Okamura), JP19H03401 (Y. Okamura), and JP19K06585 (A. Kawanabe), and Japan Science and Technology Agency CREST grant no. JPMJCR14M3 (Y. Okamura).

The authors declare no competing financial interests.

Author contributions: A. Kawanabe, N. Mizutani, O.K. Polat, and T. Yonezawa performed experiments. A. Kawanabe, T. Kawai, and O.K. Polat analyzed the data. A. Kawanabe, M.X. Mori, and Y. Okamura designed the experiments. A. Kawanabe and Y. Okamura wrote the paper.

Submitted: 17 September 2019

Revised: 5 December 2019

Accepted: 16 February 2020

## References

Balla, T. 2013. Phosphoinositides: tiny lipids with giant impact on cell regulation. *Physiol. Rev.* 93:1019–1137. <https://doi.org/10.1152/physrev.00028.2012>

Falkenburger, B.H., J.B. Jensen, and B. Hille. 2010. Kinetics of PIP<sub>2</sub> metabolism and KCNQ2/3 channel regulation studied with a voltage-sensitive phosphatase in living cells. *J. Gen. Physiol.* 135:99–114. <https://doi.org/10.1085/jgp.200910345>

Hille, B. 2001. Ion channels of excitable membranes. Sinauer, Sunderland, MA. 814 pp.

Hille, B., E.J. Dickson, M. Kruse, O. Vivas, and B.C. Suh. 2015. Phosphoinositides regulate ion channels. *Biochim. Biophys. Acta.* 1851:844–856. <https://doi.org/10.1016/j.bbaplp.2014.09.010>

Hossain, M.I., H. Iwasaki, Y. Okochi, M. Chahine, S. Higashijima, K. Nagayama, and Y. Okamura. 2008. Enzyme domain affects the movement of the voltage sensor in ascidian and zebrafish voltage-sensing phosphatases. *J. Biol. Chem.* 283:18248–18259. <https://doi.org/10.1074/jbc.M706184200>

Idevall-Hagren, O., E.J. Dickson, B. Hille, D.K. Toomre, and P. De Camilli. 2012. Optogenetic control of phosphoinositide metabolism. *Proc. Natl. Acad. Sci. USA.* 109:E2316–E2323. <https://doi.org/10.1073/pnas.1211305109>

Imai, Y., K. Itsuki, Y. Okamura, R. Inoue, and M.X. Mori. 2012. A self-limiting regulation of vasoconstrictor-activated TRPC3/C6/C7 channels coupled to PI(4,5)P<sub>2</sub>-diacylglycerol signalling. *J. Physiol.* 590:1101–1119. <https://doi.org/10.1113/jphysiol.2011.221358>

Itsuki, K., Y. Imai, Y. Okamura, K. Abe, R. Inoue, and M.X. Mori. 2012. Voltage-sensing phosphatase reveals temporal regulation of TRPC3/C6/C7 channels by membrane phosphoinositides. *Channels (Austin).* 6: 206–209. <https://doi.org/10.4161/chan.20883>

Kawanabe, A., M. Hashimoto, M. Nishizawa, K. Nishizawa, H. Narita, T. Yonezawa, Y. Jinno, S. Sakata, A. Nakagawa, and Y. Okamura. 2018. The hydrophobic nature of a novel membrane interface regulates the enzyme activity of a voltage-sensing phosphatase. *eLife.* 7:e41653. <https://doi.org/10.7554/eLife.41653>

Keum, D., M. Kruse, D.I. Kim, B. Hille, and B.C. Suh. 2016. Phosphoinositide 5- and 3-phosphatase activities of a voltage-sensing phosphatase in living cells show identical voltage dependence. *Proc. Natl. Acad. Sci. USA.* 113: E3686–E3695. <https://doi.org/10.1073/pnas.1606472113>

Kruse, M., G.R. Hammond, and B. Hille. 2012. Regulation of voltage-gated potassium channels by PI(4,5)P<sub>2</sub>. *J. Gen. Physiol.* 140:189–205. <https://doi.org/10.1085/jgp.201210806>

Laverty, D., R. Desai, T. Uchański, S. Masiulis, W.J. Stec, T. Malinauskas, J. Zivanov, E. Pardon, J. Steyaert, K.W. Miller, and A.R. Aricescu. 2019. Cryo-EM structure of the human  $\alpha 1\beta 3\gamma 2$  GABA<sub>A</sub> receptor in a lipid bilayer. *Nature.* 565:516–520. <https://doi.org/10.1038/s41586-018-0833-4>

Mennerick, S., A.A. Taylor, and C.F. Zorumski. 2014. Phosphatidylinositol 4,5-bisphosphate depletion fails to affect neurosteroid modulation of GABA<sub>A</sub> receptor function. *Psychopharmacology (Berl.).* 231:3493–3501. <https://doi.org/10.1007/s00213-014-3486-5>

Mizutani, N., Y. Okochi, and Y. Okamura. 2019. Distinct functional properties of two electrogenic isoforms of the SLC34 Na-Pi cotransporter. *Physiol. Rep.* 7:e14156. <https://doi.org/10.14814/phy2.14156>

Murata, Y., and Y. Okamura. 2007. Depolarization activates the phosphoinositide phosphatase Ci-VSP, as detected in *Xenopus* oocytes coexpressing sensors of PIP<sub>2</sub>. *J. Physiol.* 583:875–889. <https://doi.org/10.1113/jphysiol.2007.134775>

Okamura, Y., Y. Murata, and H. Iwasaki. 2009. Voltage-sensing phosphatase: actions and potentials. *J. Physiol.* 587:513–520. <https://doi.org/10.1113/jphysiol.2008.163097>

Okamura, Y., A. Kawanabe, and T. Kawai. 2018. Voltage-sensing phosphatases: biophysics, physiology and molecular engineering. *Physiol. Rev.* 98:2097–2131. <https://doi.org/10.1152/physrev.00056.2017>

Rayaprolu, V., P. Royal, K. Stengel, G. Sandoz, and S.C. Kohout. 2018. Dimerization of the voltage-sensing phosphatase controls its voltage-sensing and catalytic activity. *J. Gen. Physiol.* 150:683–696. <https://doi.org/10.1085/jgp.201812064>

Rjasanow, A., M.G. Leitner, V. Thallmair, C.R. Halaszovich, and D. Oliver. 2015. Ion channel regulation by phosphoinositides analyzed with VSPs-PI(4,5)P<sub>2</sub> affinity, phosphoinositide selectivity, and PI(4,5)P<sub>2</sub> pool accessibility. *Front. Pharmacol.* 6:127. <https://doi.org/10.3389/fphar.2015.00127>

Sakata, S., and Y. Okamura. 2014. Phosphatase activity of the voltage-sensing phosphatase, VSP, shows graded dependence on the extent of activation of the voltage sensor. *J. Physiol.* 592:899–914. <https://doi.org/10.1113/jphysiol.2013.263640>

Sakata, S., M.I. Hossain, and Y. Okamura. 2011. Coupling of the phosphatase activity of Ci-VSP to its voltage sensor activity over the entire range of voltage sensitivity. *J. Physiol.* 589:2687–2705. <https://doi.org/10.1113/jphysiol.2011.208165>

Samie, M., X. Wang, X. Zhang, A. Goschka, X. Li, X. Cheng, E. Gregg, M. Azar, Y. Zhuo, A.G. Garrity, et al. 2013. A TRP channel in the lysosome regulates large particle phagocytosis via focal exocytosis. *Dev. Cell.* 26: 511–524. <https://doi.org/10.1016/j.devcel.2013.08.003>

She, J., W. Zeng, J. Guo, Q. Chen, X.C. Bai, and Y. Jiang. 2019. Structural mechanisms of phospholipid activation of the human TPC2 channel. *eLife.* 8:e45222. <https://doi.org/10.7554/eLife.45222>

- Shimomura, T., and Y. Kubo. 2019. Phosphoinositides modulate the voltage dependence of two-pore channel 3. *J. Gen. Physiol.* 151:986–1006. <https://doi.org/10.1085/jgp.201812285>
- Suh, B.C., and B. Hille. 2005. Regulation of ion channels by phosphatidylinositol 4,5-bisphosphate. *Curr. Opin. Neurobiol.* 15:370–378. <https://doi.org/10.1016/j.conb.2005.05.005>
- Suh, B.C., K. Leal, and B. Hille. 2010. Modulation of high-voltage activated Ca(2+) channels by membrane phosphatidylinositol 4,5-bisphosphate. *Neuron.* 67:224–238. <https://doi.org/10.1016/j.neuron.2010.07.001>
- Tang, Q.Y., T. Larry, K. Hendra, E. Yamamoto, J. Bell, M. Cui, D.E. Logothetis, and L.M. Boland. 2015. Mutations in nature conferred a high affinity phosphatidylinositol 4,5-bisphosphate-binding site in vertebrate inwardly rectifying potassium channels. *J. Biol. Chem.* 290:16517–16529. <https://doi.org/10.1074/jbc.M115.640409>
- Thornell, I.M., and M.O. Bevensee. 2015. Phosphatidylinositol 4,5-bisphosphate degradation inhibits the Na<sup>+</sup>/bicarbonate cotransporter NBCe1-B and -C variants expressed in *Xenopus* oocytes. *J. Physiol.* 593: 541–558. <https://doi.org/10.1113/jphysiol.2014.284307>
- Tsutsui, H., Y. Jinno, A. Tomita, Y. Niino, Y. Yamada, K. Mikoshiba, A. Miyawaki, and Y. Okamura. 2013. Improved detection of electrical activity with a voltage probe based on a voltage-sensing phosphatase. *J. Physiol.* 591:4427–4437. <https://doi.org/10.1113/jphysiol.2013.257048>